Research Article GU J Sci, Part A, 13(1): 146-164 (2026) 10.54287/gujsa.1813548

Gazi University
Journal of Science
PART A: ENGINEERING AND INNOVATION
http://dergipark.org.tr/gujsa

The Experimental Study of Bi-directional Buck-Boost Converter Based on GaN-FETs for Satellite Energy Systems

Ahmet KARAARSLAN[1*] Hüseyin URAL[1]

[1] Ankara Yıldırım Beyazıt University, Department of Electrical and Electronics Engineering, Ankara, Türkiye

Keywords

High Power Density
Bi-directional Buck-Boost Converter
GaN-FETs
Satellite Energy Systems

Abstract

This study presents the design and experimental validation of a bi-directional, non-inverting Buck–Boost DC–DC converter based on Gallium Nitride (GaN) field-effect transistors for satellite power management and distribution systems. The symmetrical topology enables fully bi-directional power flow, supporting charging and discharging operations in distributed spacecraft power architectures. GaN devices enable high-frequency operation up to 500 kHz, reducing switching losses and allowing a compact, high–power-density implementation. The converter is designed in alignment with key ECSS-E-ST-20C guidelines adopted by the European Space Agency (ESA), including component derating, protection strategies, and thermal margin considerations, while full ECSS qualification and ESA acceptance testing are beyond the scope of this work. Active current and voltage protection mechanisms are incorporated to ensure safe operation under wide input-voltage variations and dynamic load conditions. Experimental results demonstrate a rated output power of 90 W, a maximum output power of 135 W, a peak efficiency of 95.2%, a power density of 375 W/cm³, and a maximum device temperature below 73 °C at full load under ambient laboratory conditions. The results indicate that the proposed GaN-based converter is a promising candidate architecture for future ESA-aligned, ECSS-compliant satellite power processing units.

Cite

Karaarslan, A., & Ural, H. (2026). The Experimental Study of Bi-directional Buck-Boost Converter Based on GaN-FETs for Satellite Energy Systems. *GU J Sci, Part A*, *13*(1), 146-164. doi:10.54287/gujsa.1813548

Author ID (ORCID Number)

0000-0001-6475-4539 Ahmet KARAARSLAN
0009-0003-0724-8068 Hüseyin URAL

Article Process

Submission Date 30.10.2025
Revision Date 30.12.2025
Accepted Date 12.03.2026
Published Date 31.03.2026

1. INTRODUCTION

In recent years, the demand for more efficient and compact power electronic systems has catalyzed advancements in semiconductor materials and topologies for DC-DC converters. Among these developments, Gallium Nitride (GaN) technology has emerged as a pivotal innovation, transforming the field of power electronics. The unique material properties of GaN, such as its high electron mobility and superior breakdown voltage, make GaN-based Field Effect Transistors (GaN-FETs) ideal candidates for high-frequency and high-efficiency power conversion applications (Colino & Beach, 2009; Anuraag et al., 2021).

One of the most promising implementations of GaN-FET technology is in DC-DC converters, particularly in bi-directional non-inverting buck-boost configurations. These converters play a critical role in enabling voltage regulation and energy transfer across a wide input–output range, which is essential for systems requiring both

*Corresponding Author, e-mail: akaraarslan@aybu.edu.tr

step-up and step-down conversion modes (Midya et al., 2004; Shoihet & Slonim, 2012; An & Lu, 2015). The integration of GaN-FETs in these architectures facilitates high switching frequencies with reduced losses, resulting in higher power density and smaller passive components (Tsai & Tsai, 2014; Veerachary, 2024).

The importance of small-sized, high-efficiency DC-DC converters continues to grow across modern electronic systems (Wang et al., 2023). Compact converters contribute to the miniaturization and performance enhancement of smartphones, laptops, wearable medical sensors, and Internet of Things (IoT) devices, where efficiency, thermal management, and form factor are tightly constrained (Prodic & Maksimovic, 2002; Agamy et al., 2013; Khuntia & Veerachary, 2024). The ability of these converters to efficiently regulate and convert voltage levels in limited space has positioned them as key enablers in energy-efficient product design (Zhang et al., 2008; Luo & Ma, 2010; Abdelmessih et al., 2020; Park et al., 2023).

The non-inverting buck-boost converter is particularly valuable due to its ability to manage dynamic input and output conditions while maintaining stable regulation (Ullah et al., 2022). This feature makes it especially suitable for applications involving variable power sources—such as renewable energy systems—or dynamic load environments like battery management and electric mobility systems (Wai & Shih, 2011; Chan, 2024).

In the context of satellite and space applications, these characteristics gain additional importance. Spaceborne power processing units (PPUs) and electrical power subsystems (EPS) demand converters that exhibit high efficiency, wide voltage adaptability, low mass, and robust thermal performance under harsh environmental conditions (Paul & Maksimovic, 2008; Luo et al., 2022). GaN-FET-based converters, due to their radiation tolerance and superior thermal behavior, offer a compelling solution for such environments (Fleetwood et al., 2022). Moreover, compliance with ECSS-E-ST-20C—the European Cooperation for Space Standardization guideline for electrical and electronic subsystems—is essential to ensure that converters meet stringent design, derating, and verification requirements for space qualification (Turriate, 2018). Ensuring ECSS compliance not only validates the converter's functional and environmental robustness but also facilitates its integration into European Space Agency (ESA) flight hardware and mission architectures (ESA, 2023).

This paper presents the design and implementation of a bi-directional, GaN-FET-based non-inverting buck-boost converter featuring high power density and efficient operation in Continuous Conduction Mode (CCM) at 135 W. Section 2 outlines the key design parameters and operational modes of the converter in CCM. Section 3 introduces the proposed control methodology. Sections 4 and 5 discuss the converter's performance through both simulation and experimental validation. Finally, Section 6 concludes the study, highlighting the converter's suitability for ECSS-compliant satellite power systems.

2. CIRCUIT DESCRIPTION AND OPERATION

The bi-directional non-inverting buck–boost converter can be conceptually regarded as an integration of conventional buck and boost converter stages, as illustrated in Figure 1. The topology comprises two principal

sections: a buck stage that steps down the input voltage and a boost stage that subsequently elevates this intermediate voltage to the required output level. For improved efficiency and reliability, active switches Q_2 and Q_3 are employed in place of conventional diodes, thereby reducing conduction losses and enabling efficient bidirectional power flow. In the context of space power systems, this configuration offers enhanced energy transfer capability between different voltage domains, supporting both charging and discharging modes in energy storage subsystems. Furthermore, the converter's architecture adheres to the design principles and reliability criteria defined in ECSS-E-ST-20C, ensuring compliance with space-grade electrical performance, thermal management, and electromagnetic compatibility requirements essential for high-reliability missions.

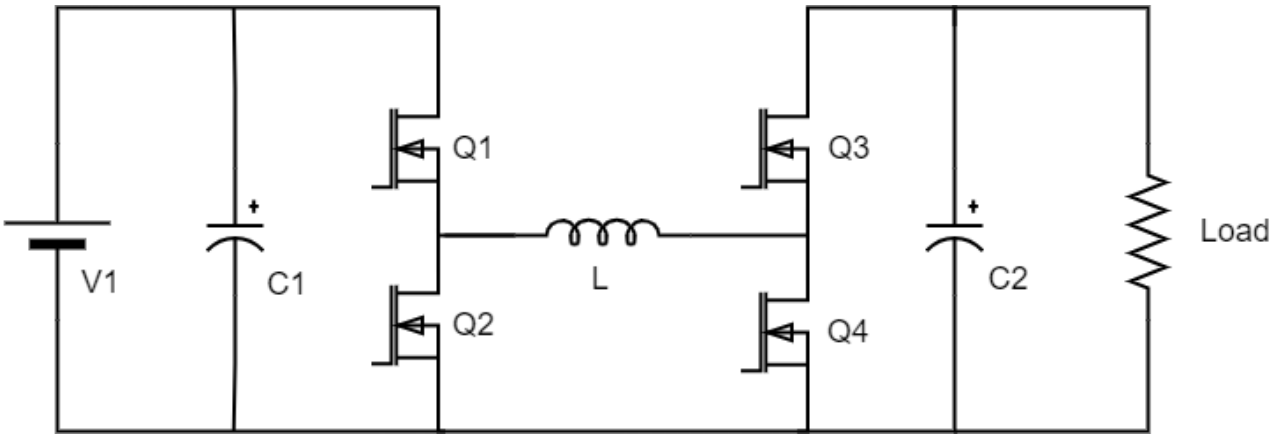

Figure 1. *Bi-directional Non-Inverting Buck Boost Converter Topology*

2.1. Buck Mode Operation

In the buck mode operation, the converter operates through two primary stages: the inductor charging stage and the inductor discharging stages showing the key switching transitions and energy transfer paths. This controlled two-stage operation ensures stable voltage regulation and minimized switching stress for electrical performance and reliability in space power conditioning systems.

Buck Stage 1: In the initial stage that is given in Figure 2, switches Q_1 and Q_3 are activated, whereas Q_2 and Q_4 are turned off. During this period, the inductor L is energized, storing magnetic energy derived from the input source. The voltage drop across L and the resulting output voltage behavior are described by the following equations.

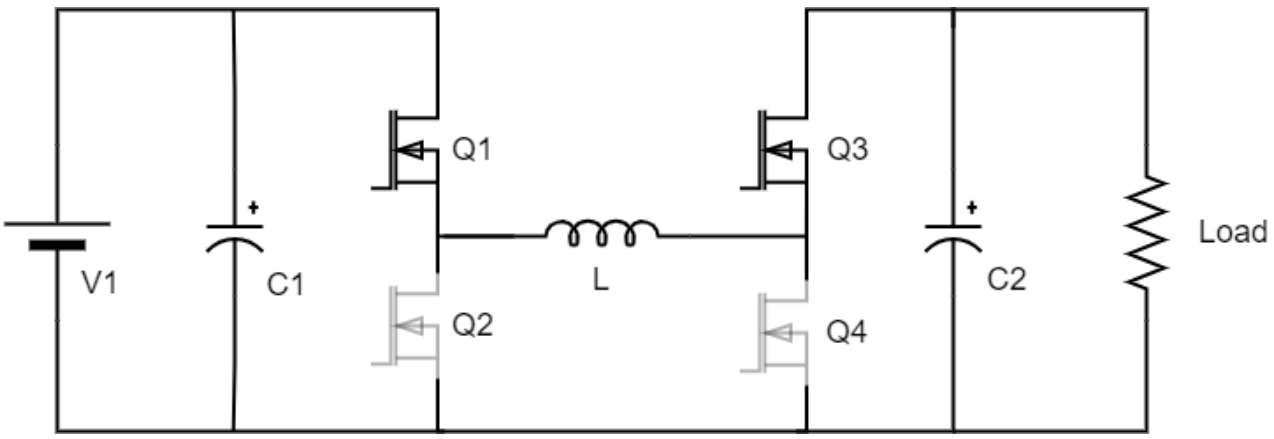

Figure 2. *Operation of Buck Stage1*

$$V_{L1} = L_1 * \frac{di}{dt} \quad (1)$$

$$V_{OUT} = V_{IN} - V_{L1} \quad (2)$$

Buck Stage 2: In Stage 2 that is given in Figure 3, switches Q_2 and Q_3 are activated, whereas Q_1 and Q_4 are turned off. The inductor L, previously charged during Stage 1, reverses its polarity and releases stored energy to maintain the required output voltage. During this phase, the output power is sustained by both the inductor L and the output capacitor C_2, ensuring continuous load current and voltage stability. The voltage developed across L and the resulting output voltage behavior are represented by the following equations.

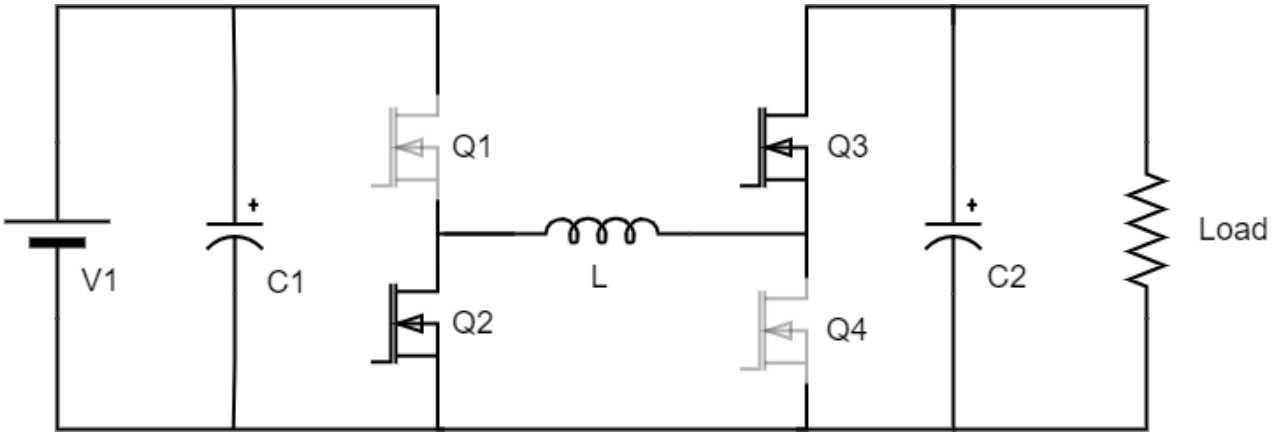

Figure 3. *Operation of Buck Stage2*

$$V_{L1} = V_{OUT} \quad (3)$$

$$V_{L1} = L * \frac{di}{per(1-D)} \quad (4)$$

Substitute Equation (4) in Equation (3)

$$di = V_{OUT} \frac{per(1-D)}{L} \quad (5)$$

To calculate relation between inductor voltage, output voltage and duty substitute Equation (5) in Equation (3).

$$V_{L1} = V_{OUT} \frac{1-D}{D} \quad (6)$$

To calculate input voltage, output voltage and duty relation for buck mode substitute Equation (6) in Equation (2);

$$V_{OUT} = V_{IN} * D \quad (7)$$

During the buck operation, switch Q_4 remains off, while switch Q_3 is kept on. The primary purpose of turning on Q_3 is to eliminate the forward voltage drop across its body diode, thereby reducing conduction losses and enhancing the overall efficiency of the converter.

2.2. Boost Mode Operation

In the boost-mode operation, the converter elevates the input voltage to meet the required output level through a controlled two-stage process. The boost mode of the circuit consists of 2 stages: inductor charging stage and discharge stage.

Boost Stage 1: During the inductor charging phase that is given in Figure 4, switches Q_1 and Q_4 are activated, allowing the inductor L to store energy from the input source. In the discharging phase, switches Q_1 and Q_4 are turned off, and Q_2 and Q_3 are turned on, enabling the inductor L to release stored energy to the output capacitor C_2 and the load. This sequential switching mechanism provides efficient voltage step-up conversion with reduced ripple and controlled current transitions.

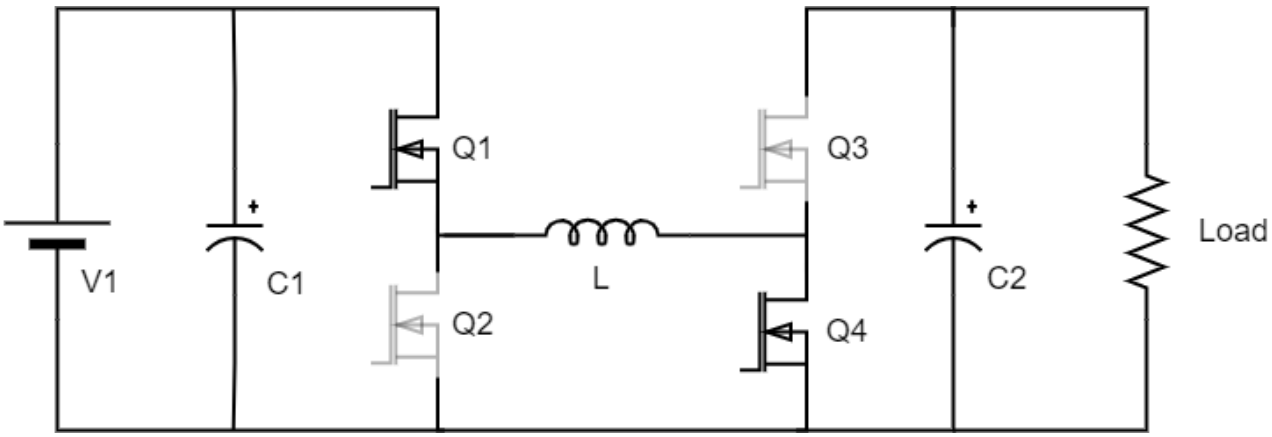

Figure 4. *Operation of Boost Stage1*

$$V_{L1} = L_1 \frac{di}{dt} \tag{8}$$

$$V_{L1} = V_{IN} \tag{9}$$

Boost Stage 2: In Stage 2 of the boost-mode operation that is given in Figure 5, switches Q_1 and Q_3 are activated, whereas Q_2 and Q_4 are turned off. The inductor L, previously energized during Stage 1, reverses its polarity and becomes connected in series with the input source. The combined voltage of the input and the inductor thus delivers the required boosted output voltage. During this period, energy is transferred from both the inductor L and the output capacitor C_2 to the load, ensuring continuous power delivery and stable voltage regulation. The voltage contribution from L and the output voltage relationship are defined by the following equations.

$$V_{OUT} = V_{IN} + V_{L1} \tag{10}$$

To calculate the relation between input voltage, output voltage and duty for boost operation, substitute Equation (9) in Equation (8) and Equation (8) in Equation (10);

$$V_{OUT} = \frac{V_{IN}}{1 - D} \tag{11}$$

The converter's operation ensures efficient bidirectional power transfer, reduced conduction and switching losses, and minimized voltage ripple — characteristics essential for high-reliability space power conditioning

systems. The design approach adheres to ECSS-E-ST-20C requirements for electrical and electronic subsystems, addressing key parameters such as thermal management, electromagnetic compatibility (EMC), and fault tolerance. By employing wide-bandgap semiconductor switches and optimized gate-drive timing, the converter achieves improved efficiency and robustness under varying load and temperature conditions typical of spacecraft environments.

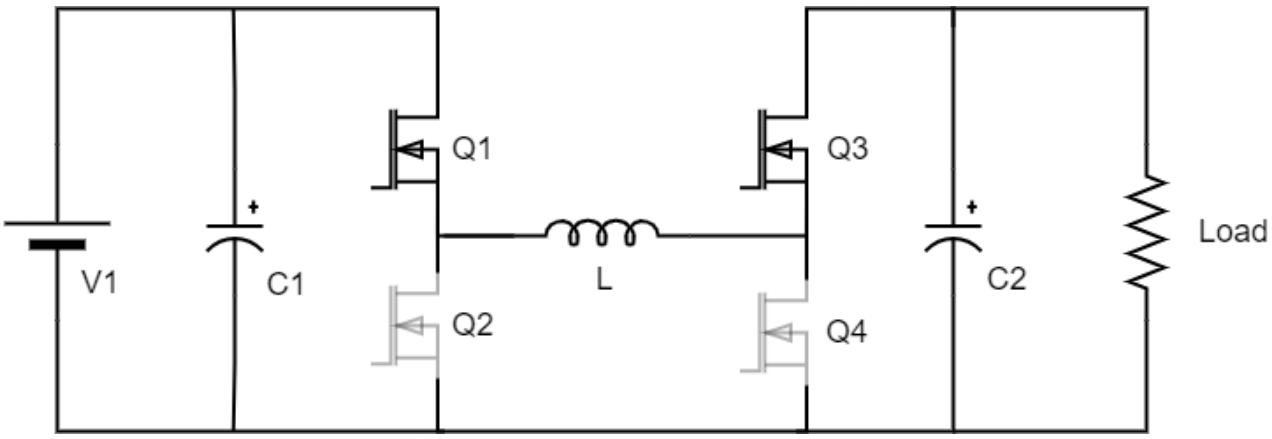

Figure 5. *Operation of Boost Stage2*

2.3. Component Sizing and Calculation

Recent developments in wide-bandgap semiconductor devices have facilitated operation at higher switching frequencies, improving power density and allowing component miniaturization. For the proposed converter, a switching frequency of 500 kHz is employed. This high-frequency operation reduces the size of passive elements, contributing to a more compact and lightweight module suitable for spaceborne applications. The inductor L is designed to maintain a 25% peak-to-peak ripple of the maximum current (4 A for a 16 A maximum), ensuring stable operation under high-current conditions. The design targets a maximum output voltage of 40 V with a minimum input voltage of 10 V, corresponding to the operational condition where the converter steps up from 10 V input to 40 V output. This configuration supports the high-reliability and efficiency requirements for spacecraft power electronics.

$$40 = \frac{10}{1-D} \Rightarrow D = 0.75 \tag{12}$$

Substitute these values in Equation (8) and Equation (9)

$$4 = 10\frac{\frac{1}{500 * 10^3}(1-0.75)}{L} \Rightarrow L = 3.75uH \tag{13}$$

The closest commonly used value for inductor, 4.7 uH is selected for simulation. C_1 is selected for 1V voltage ripple or less;

$$dV = \frac{dt * I_{OUT}}{C_1} \tag{14}$$

$$C_1 = \frac{per * D * I_{out}}{dV} \tag{15}$$

$$C_1 = \frac{\frac{1}{500 * 10^3} * 0.25 * 40}{1} \Rightarrow C = 20uF \tag{16}$$

The closest commonly used value for capacitor, C_1 "22uF" is selected for simulation and experimental studies.

3. CONTROL METHOD OF PROPOSED TOPOLOGY

A bidirectional DC–DC converter that is given in Figure 6 provides reliable and controlled energy transfer between two DC voltage domains, supporting both step-up (boost) and step-down (buck) operation. This capability is essential for spaceborne power systems, including battery management, energy storage units, and photovoltaic arrays, where efficient bidirectional energy flow is critical. The converter employs a PI (Proportional–Integral) controller to regulate the output voltage and enforce output current limits. The controller calculates the error between the reference and measured output voltages, multiplies it by a proportional gain (K_p), integrates it with an integral gain (K_i), and sums these contributions. The resulting signal passes through a saturation block that constrains the current to defined limits. If the current exceeds the saturation range, the PI output is limited, thereby reducing the controller input and preventing excessive output voltage or current.

Bidirectional operation is governed by the relation between the commanded voltage and the load voltage: energy flows from input to output when the load voltage is below the reference, and reverses when the load voltage exceeds the reference. This mechanism enables efficient and reliable power management in spacecraft systems, considering with ECSS-E-ST-20C requirements for electrical performance, voltage regulation, and load protection under varying operating conditions.

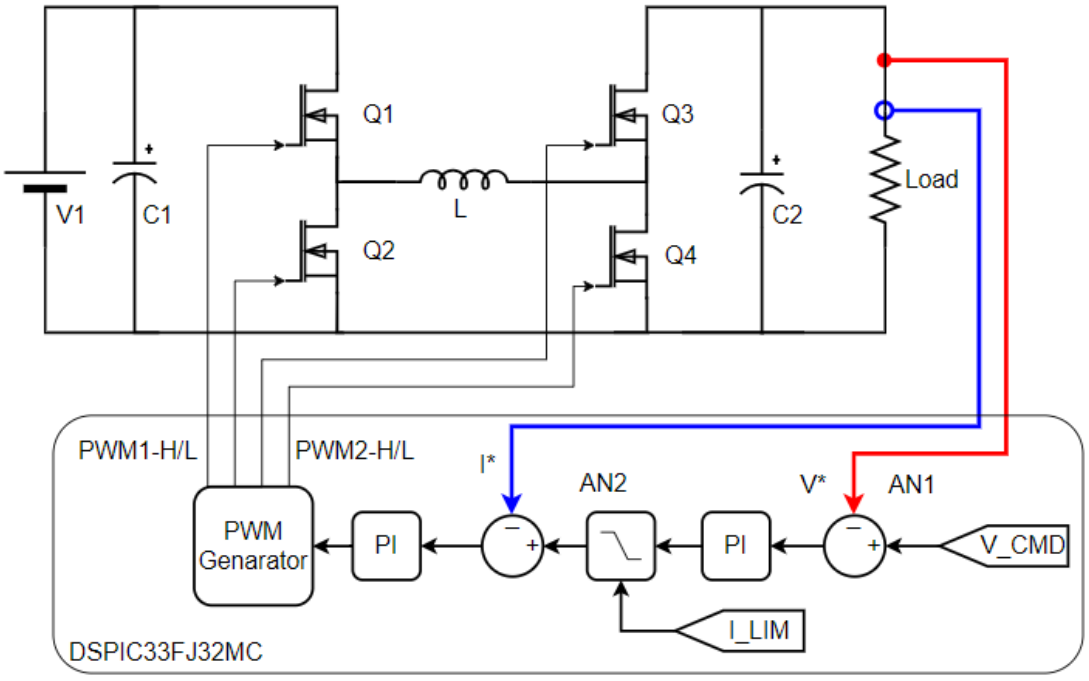

Figure 6. *Block Diagram of Control strategy of Proposed Topology*

The PI controller output is constrained between 0% and 170%, allowing a single control loop to govern both buck and boost operation, thereby simplifying the control architecture for space applications. The controller output is directly applied to the duty-cycle input of the buck converter. In buck operation, the converter reaches

input saturation at 95% duty, whereas in boost operation, saturation occurs when the PI output falls below 95%. For PI outputs above 95%, the boost converter duty is reduced, providing precise regulation of the output current. This control strategy ensures smooth mode transitions, prevents overcurrent conditions, and maintains stable voltage and current delivery for reliability, transient response, and fault-tolerant operation in spacecraft power systems.

As shown in Figure 7, the system consists of an input voltage source, followed by the previously described non-inverting buck–boost converter, and a load. The load comprises two elements: a fixed resistor and an adjustable voltage source. The adjustable source models a dynamic load that can both consume and supply energy. For example, in the context of an electric vehicle, the load consumes energy from the batteries during acceleration and returns energy to the system during regenerative braking. The resistor represents the inherent system impedance, capturing resistive losses and contributing to realistic load behavior. This configuration enables accurate simulation of bidirectional power flow under varying operating conditions.

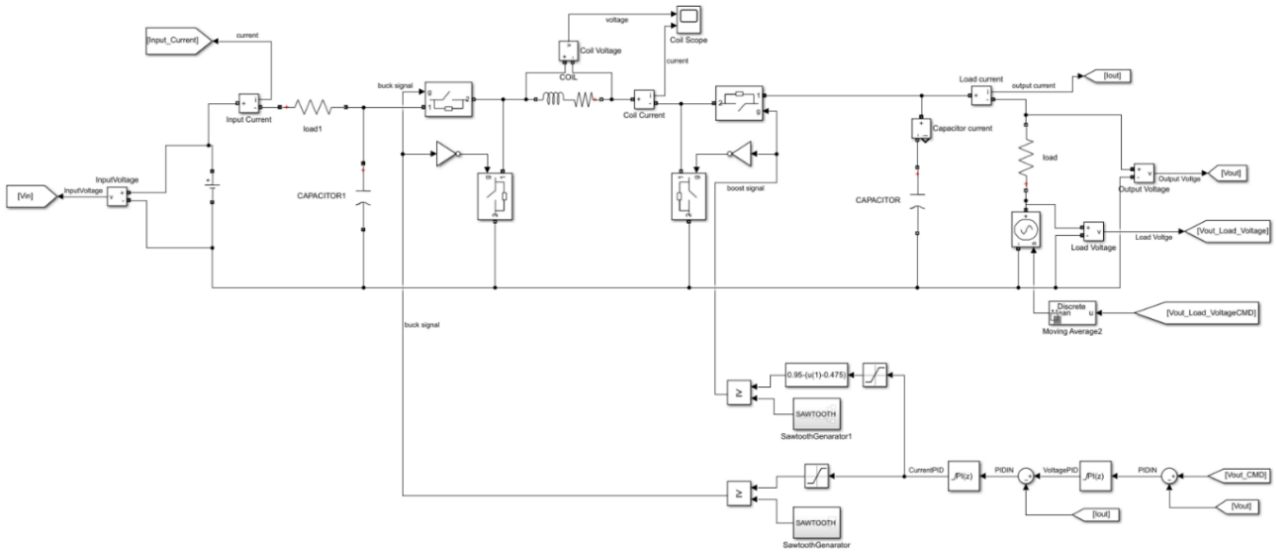

Figure 7. *Implementation of Control Method to Proposed Topology*

4. SIMULATION STUDIES OF PROPOSED CONVERTER

The control block of simulation circuit given in Figure 8 is positioned below the power stage components. PWM signals are generated for the high-side switches, while the signals for the low-side switches are obtained by inverting the corresponding high-side PWM signals. This arrangement ensures proper complementary switching and prevents shoot-through, enabling accurate representation of the converter's operation in simulation.

The simulation results shown in Figure 9 indicates the converter's response to rapid input voltage variations and output voltage regulation performance. The input voltage rise time is shorter than 10 ms, corresponding to a slew rate of 300 V/s. The converter maintains output voltage ripple below 10%, demonstrating robust handling of fast transients. When the reference output voltage is changed, the actual output voltage closely follows the command signal. Additionally, mode transitions between buck and boost operation occur

seamlessly without generating significant output ripple, indicating stable bidirectional operation. These results confirm that the converter meets ECSS-E-ST-20C requirements for transient response, voltage regulation, and mode-switching reliability in spaceborne power systems.

As illustrated in Figure 10, the direction of the output current is determined by the relative values of the output voltage and the load voltage. When the load voltage exceeds the output voltage, the current becomes negative, indicating that energy flows from the load back to the input. Conversely, when the output voltage is greater than the load voltage, the current is positive, meaning that energy flows from the input to the load. This behavior confirms the bidirectional functionality of the converter. The simulation results demonstrate that bidirectional operation is successfully achieved in both buck and boost modes, independent of the input voltage and without introducing significant output ripple. To evaluate this functionality, the load was modeled as a dynamic element, as showed in Figure 7, capable of both consuming and supplying energy.

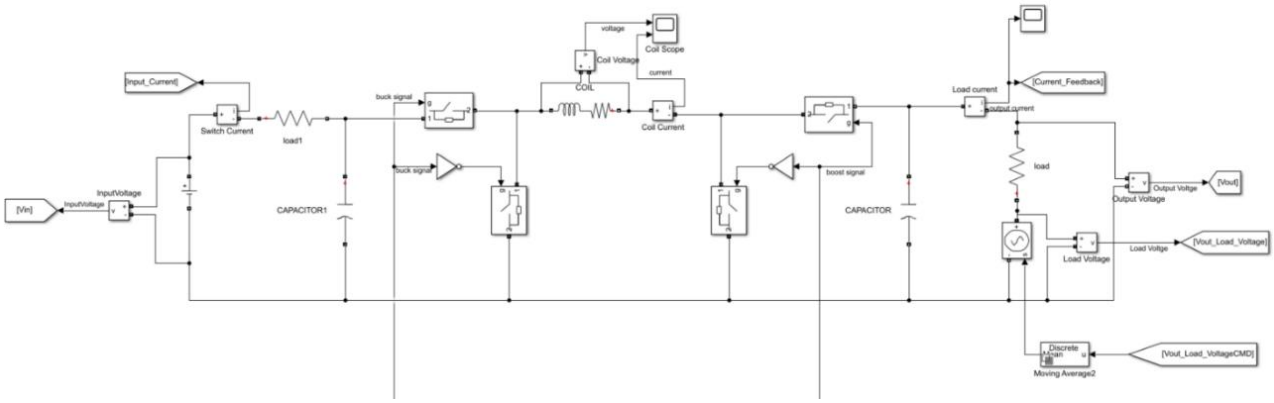

Figure 8. *Power Circuit of Matlab Simulation*

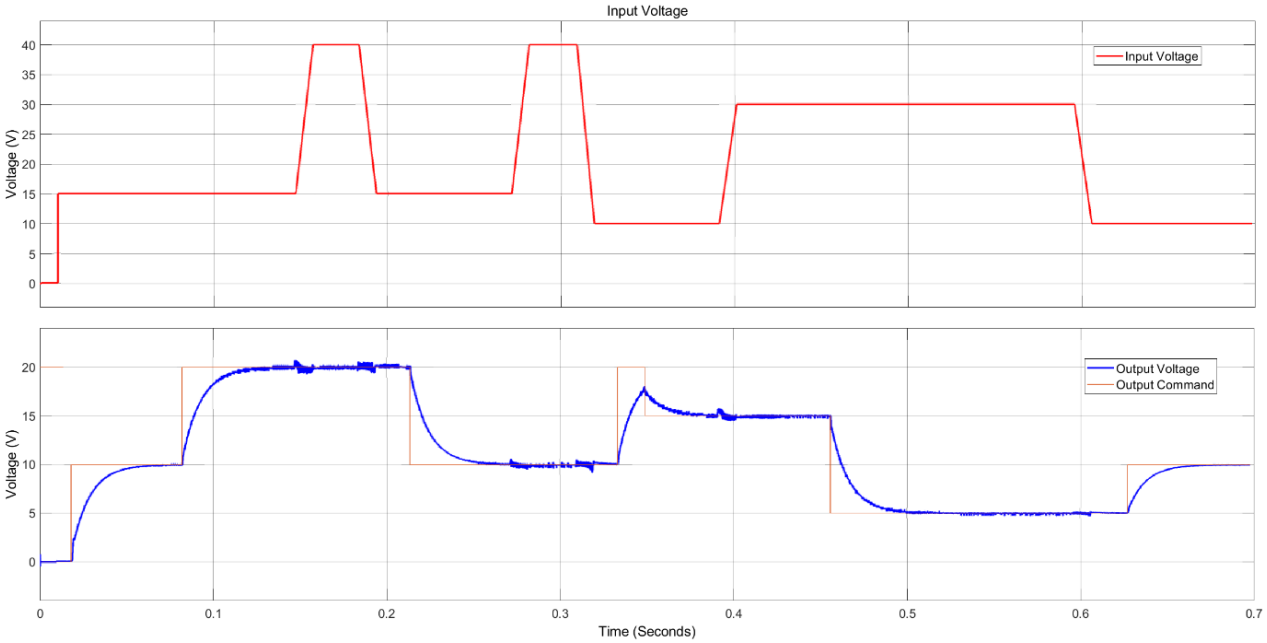

Figure 9. *Dynamic Response of Proposed Topology*

In practical space applications, high inductor current ripple that is given in Figure 11 is a significant contributor to electromagnetic interference (EMI), which can adversely affect sensitive subsystems. Simulation and theoretical analysis show that the inductor ripple current is maintained below 4 A, minimizing potential EMI. This low-ripple operation is expected to improve electromagnetic compatibility, thermal stability, and overall reliability.

The output voltage ripple, illustrated in Figure 12, remains below 1V ripple for a 40 V output, corresponding to approximately 2.5% ripple. For applications requiring higher voltage precision, the ripple can be further reduced by incorporating an additional output filter.

The simulation results clearly demonstrate that the converter is capable of regulating the output voltage across a wide range of input voltages and maintaining stable operation over various output voltage levels. In boost mode, the output voltage ripple is observed to increase slightly, which can be attributed to the inherent nonlinearity of the system.

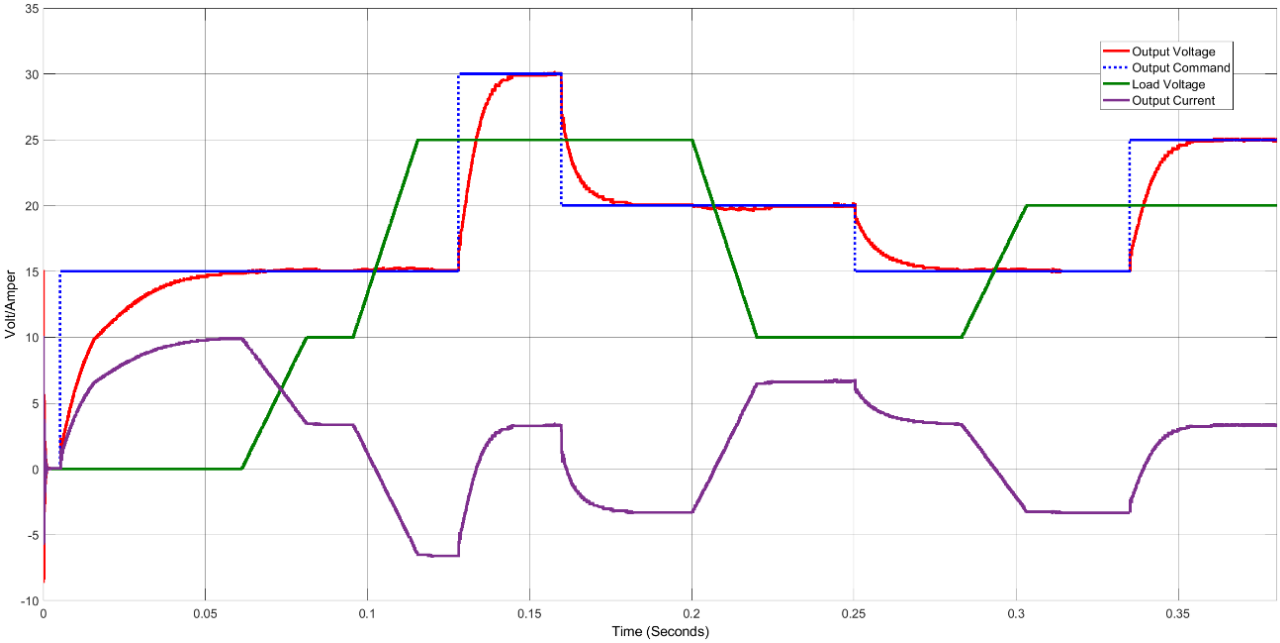

Figure 10. *Dynamic Response for Bi-directional operation*

5. EXPERIMENTAL STUDIES

This section describes the experimental evaluation of the bi-directional non-inverting buck–boost converter. The system is controlled by a dsPIC33FJ32MC MCU, which executes the PI-based control algorithm and generates the required switching signals. The MCU continuously monitors the output voltage, output current, and input voltage, providing feedback to regulate the converter similarly to the Simulink model, using identical control parameters and loop timing.

The power stage employs an H-bridge topology with four EPC2060 GaN FETs and two uP1966E GaN FET gate drivers, operating at a 500 kHz switching frequency. A dedicated LM5007 buck converter supplies the MCU and gate drivers. The experimental buck-boost converter shown in Figure 13 demonstrates the practical

implementation of high-frequency, high-efficiency operation suitable for space-qualified power electronics, in compliance with ECSS-E-ST-20C design guidelines.

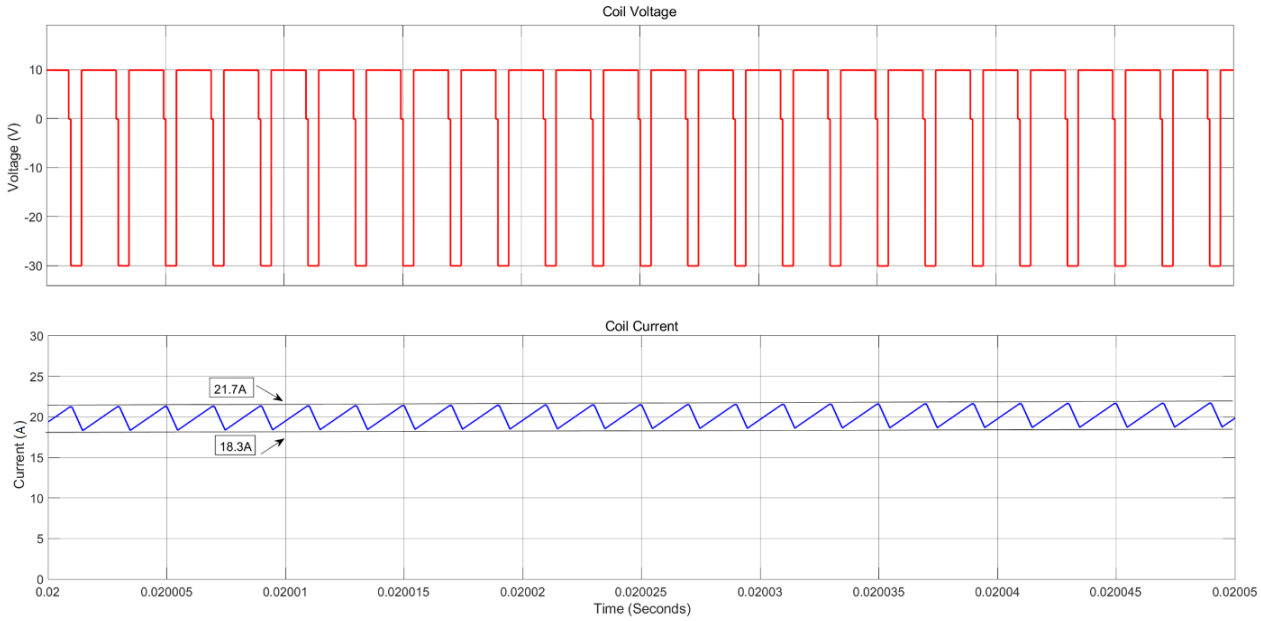

Figure 11. *Inductor Voltage and Current*

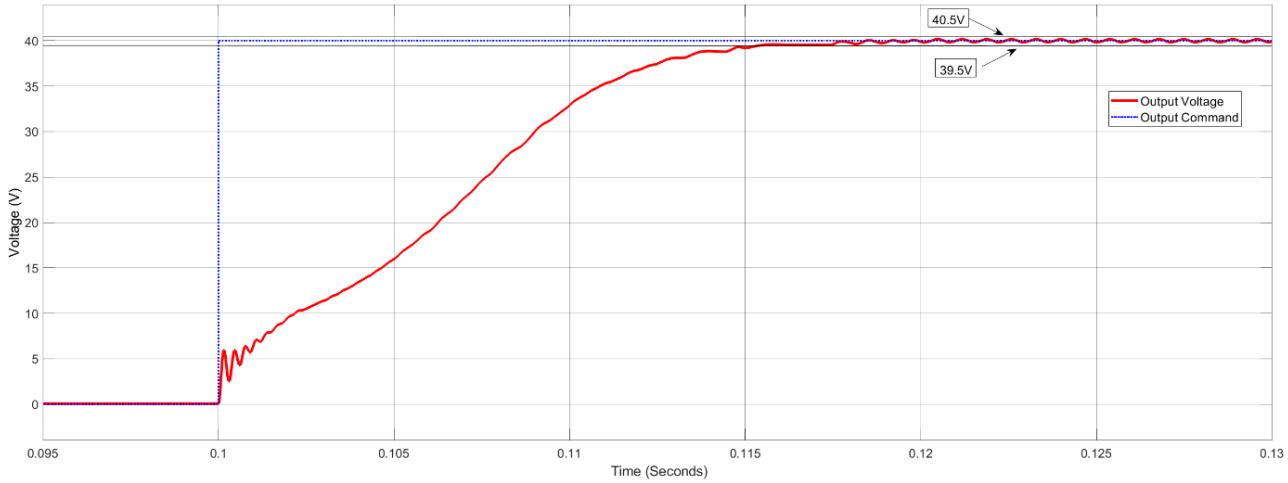

Figure 12. *Output Voltage Ripple*

The objectives of the experimental tests are as follows:

- **Thermal Performance:** The non-inverting buck–boost converter is tested under full-load conditions. Component and board temperatures are measured using thermal imaging cameras to assess heat dissipation and thermal stability.
- **Efficiency:** Input currents and voltages are measured across a range of 10V to 40V in 5V increments, while output voltage and current are recorded for fixed output references of 12V, 15V, 24V, and 30V. These measurements are used to evaluate the converter's efficiency under varying operating conditions.

- **Controller Response:** The effects of instantaneous changes in input voltage and load on the output voltage are observed to assess dynamic response and control performance.
- **Steady-State Noise:** The converter is tested at 30 V input under no-load, 4A, and 9A load conditions at a 15V constant output voltage, and steady-state output noise is recorded using an oscilloscope.
- **Start-Up Behavior:** The response of the converter during initial energization is evaluated to characterize startup transients and settling behavior.

The test setup for the bidirectional non-inverting buck–boost converter shown in Figure 14, incorporates a comprehensive suite of instruments to enable precise evaluation of the converter's performance. A programmable power supply provides accurate adjustment of input voltages to simulate various operating conditions, while an electronic load allows controlled loading of the converter to assess its response under different output conditions. A cooling fan is integrated to manage thermal considerations during full-load operation.

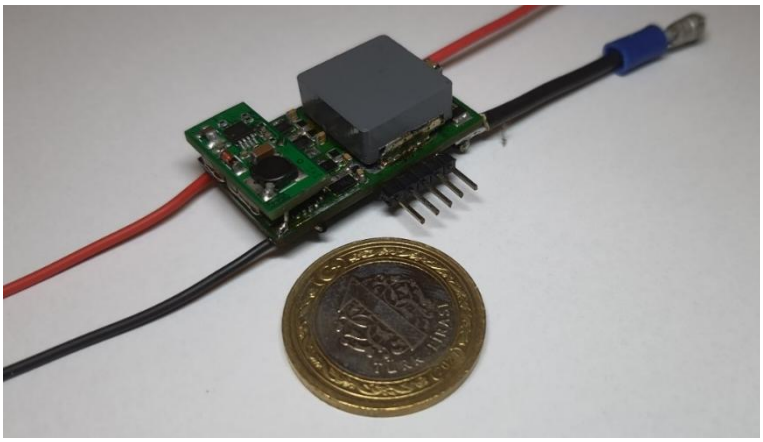

Figure 13. *Bidirectional Non-Inverting Buck-Boost Converter*

Thermal performance that is given in Figure 15 monitored using a thermal imaging camera, which captures temperature distributions across critical components. For electrical measurements, an oscilloscope with dual voltage probes is used to simultaneously record input and output voltages, and a current probe measures input and output currents with high accuracy. This comprehensive setup enables thorough characterization of the converter's electrical and thermal performance under a wide range of operating conditions.

Under challenging conditions—30 V input and 12 V, 5 A output, representing the maximum power and least efficient operating point—the non-inverting buck–boost converter exhibits effective thermal management despite relying solely on a fan-based cooling solution rather than advanced methods such as liquid cooling or cold plates. Thermal measurements show a maximum temperature of 73°C on the GaN FETs, demonstrating efficient heat dissipation. Heat is conducted away via 2 oz (70 μm) thick copper planes embedded directly beneath the FETs, maximizing thermal spreading across the PCB.

Figure 16 illustrates the measured efficiency of the proposed converter as a function of output power. The efficiency increases rapidly from approximately 85% at light load to above 90% beyond 30 W, indicating

reduced dominance of fixed losses as the load increases. A peak efficiency of about 95% is achieved around the nominal operating range of 80–100 W. At higher output power levels, a slight efficiency degradation is observed, primarily attributed to increased conduction losses and thermal effects in the power devices. Overall, the converter maintains an efficiency above 94% over a wide mid-to-high load range, demonstrating its suitability for high-efficiency satellite power management applications.

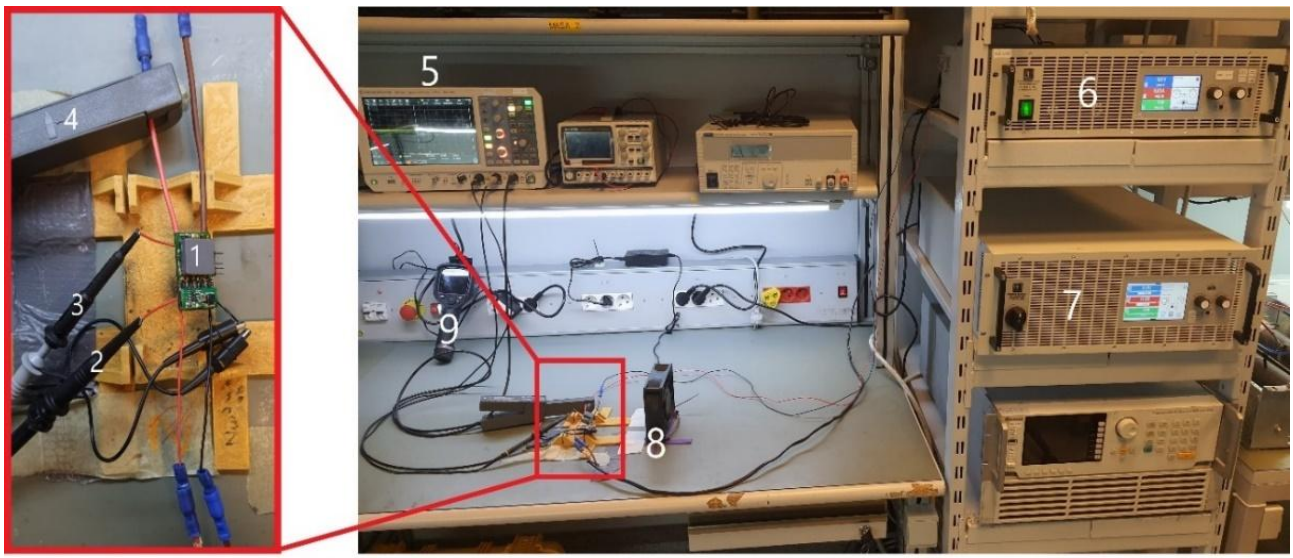

Number	Equipment
1	Non-Inverting Buck Boost Converter (Equipment Under Test)
2	Oscilloscope Voltage Probe (CH2)
3	Oscilloscope Voltage Probe (CH1)
4	Oscilloscope Current Probe (CH3)
5	Oscilloscope
6	Electronic load
7	Programmable Power Supply
8	Cooling Fan
9	Thermal Camera

Figure 14. *Test Setup of Bidirectional Non-Inverting Buck-Boost Converter*

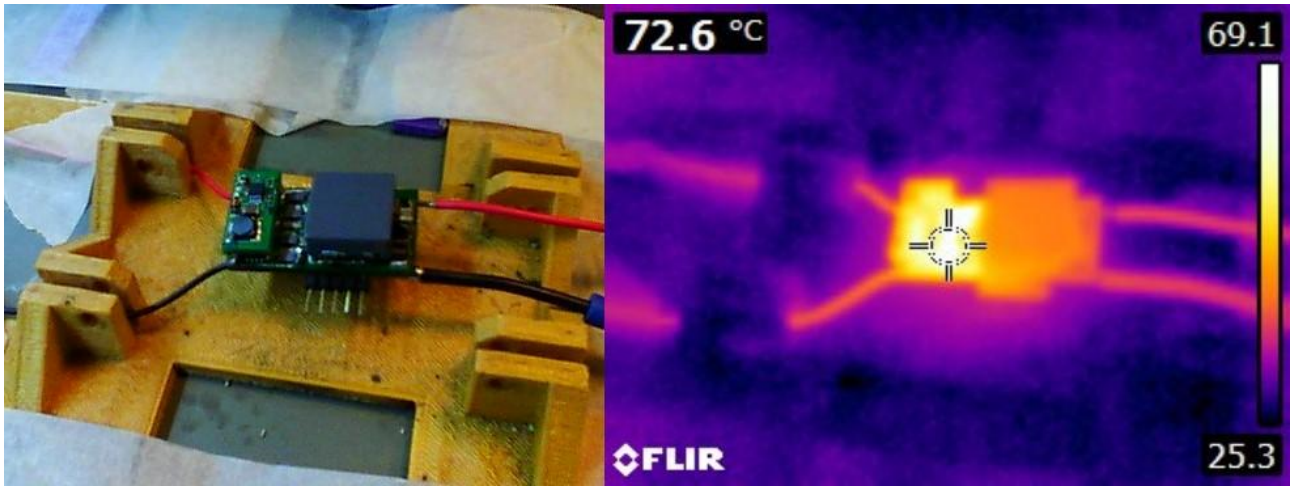

Figure 15. *Full load Thermal Measurements*

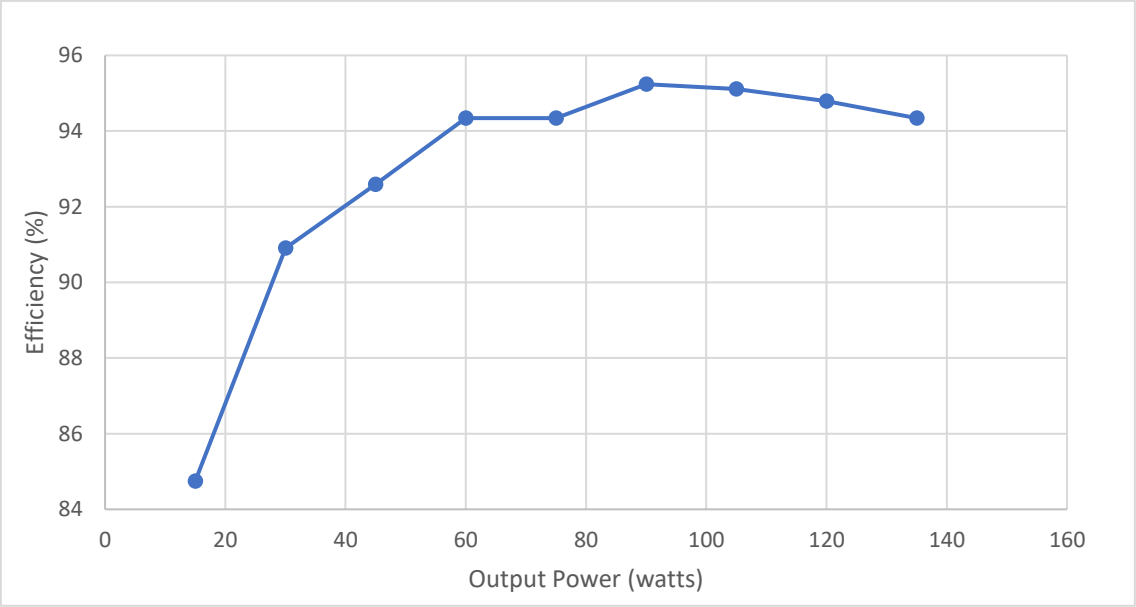

Figure 16. *Efficiency (%) vs Output Power (Watt)*

The experimental results in Figure 17 indicate that the non-inverting buck–boost converter reaches a peak efficiency of 95.2% at a 30 V input and 15 V output, with an input current of 3.15 A (input power 94.5 W) and an output of 15 V at 6 A (output power 90 W). Across a broad operational range of 60 W to 135 W, the converter maintains efficiencies exceeding 94%, highlighting its suitability for spaceborne applications where high-efficiency power conversion is critical.

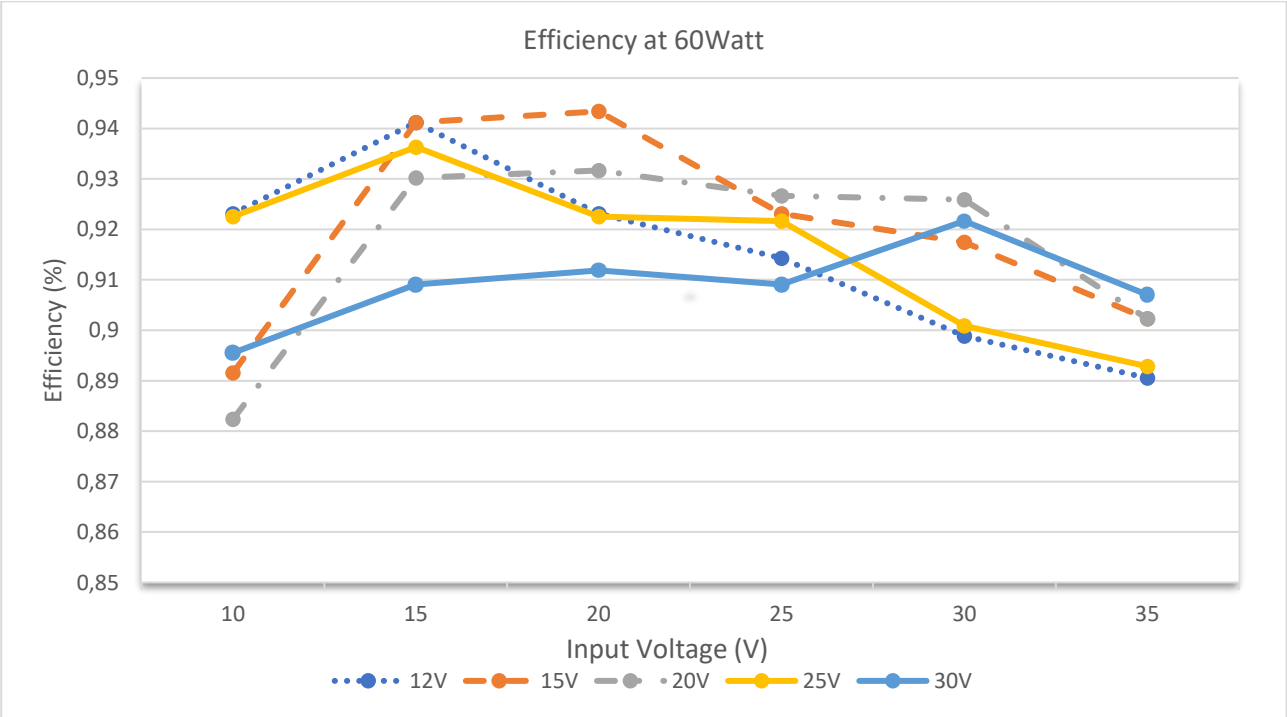

Figure 17. *Efficiency with Respect to Input and Output Voltages at 60 Watt*

The non-inverting buck–boost converter was tested to evaluate the effect of varying input and output voltages on efficiency. For a constant 12 V, 5 A output, measurements were conducted over an input voltage range of 10 V to 35 V. Input and output voltages, along with the corresponding currents, were recorded using an

oscilloscope, with results represented by dashed blue lines in Figure 15. The study was extended to additional output configurations, including 15 V at 4 A, 20 V at 3 A, 25 V at 2.4 A, and 30 V at 2 A, with each dataset recorded and illustrated in Figure 15. Data analysis revealed that the peak efficiency of 94% occurred at 15 V output, 4 A with a 20 V input. These results demonstrate the critical influence of the input–output voltage relationship on converter efficiency and emphasize the importance of optimizing voltage parameters to achieve enhanced performance.

The input voltage is supplied from a programmable voltage supply the voltage supply programmed for trapezoidal shaped voltage. The input voltage is increased from 10V to 40V in 100ms. Then the voltage decreased from 40V to 10V. The effect of the input voltage to output voltage is represented in Figure 18.

Load transients are a critical consideration for DC–DC converters in space applications. In Figure 19, the load current was increased from 0 A to 4 A over 10 ms, resulting in a temporary decrease in output voltage from 15 V to 14.649 V (ΔV = 0.351 V). When the load current decreased from 4 A to 0 A within 1 ms, the output voltage increased from 15 V to 16.553 V (ΔV = 1.553 V). These measurements demonstrate the converter's dynamic response and its ability to regulate voltage under rapid load transients

In Figure 20, the load current was increased from 0 A to 9 A within 10 ms, resulting in a decrease of the output voltage from 15 V to 13.7 V, corresponding to a drop of 1.3 V. Conversely, when the load current decreased from 9 A to 0 A within 1 ms, the output voltage increased from 15 V to 17.1 V, yielding a rise of 2.1 V. These results highlight the converter's transient response under large load changes, demonstrating its capability to maintain voltage regulation even under rapid and substantial load variations.

The start-up time of the non-inverting buck–boost converter is defined as the duration for the output voltage to reach the commanded reference. Figure 21 illustrates the start-up for a 15 V reference output at a 10 V input.

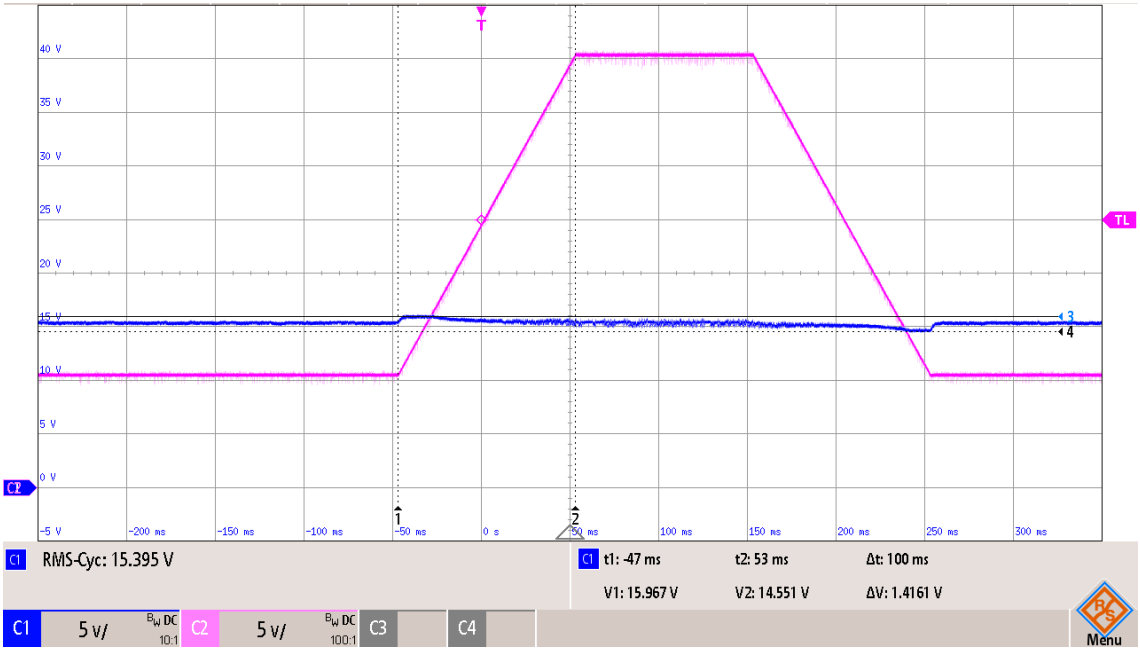

Figure 18. *Effect of Input Voltage Variation*

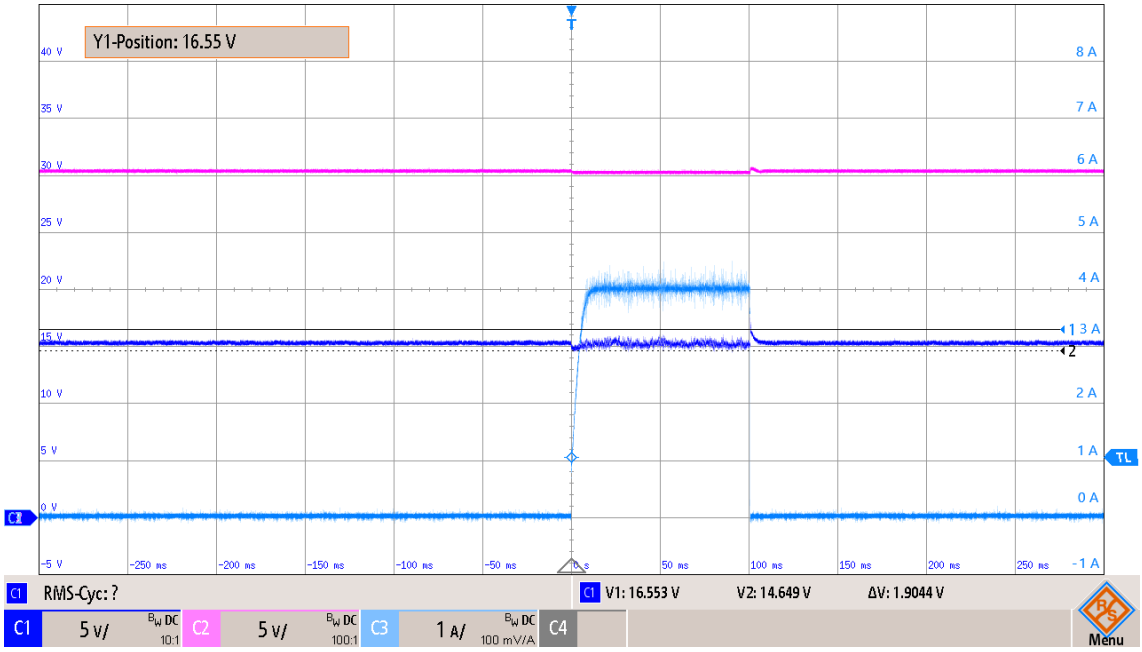

Figure 19. *Load Variation from no Load to Half Load, and Vice Versa*

The output voltage then ramps up smoothly, reaching the reference value of approximately 15 V within 5 ms, as indicated by the ΔV measurement on the oscilloscope. The voltage rise exhibits near-exponential behavior, which is typical for converters governed by control loops, reflecting the combined effects of the output filter capacitor, inductor dynamics, and controller response. Minor voltage fluctuations observed during the ramp are within acceptable limits and do not compromise regulation. Depending on the application, the start-up time can be programmed and adjusted via the control software, providing flexibility for different system requirements. These results confirm predictable and controllable start-up behavior, in alignment with ECSS-E-ST-20C requirements for spaceborne power systems.

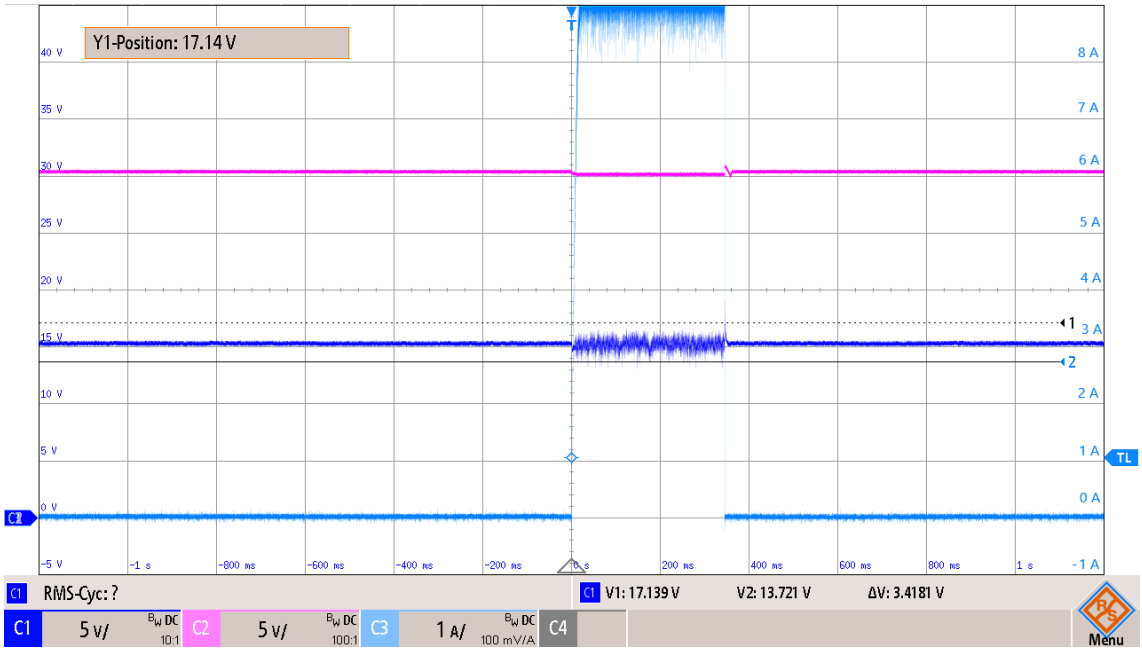

Figure 20. *Load Variation from No Load to Full Load, and Vice Versa*

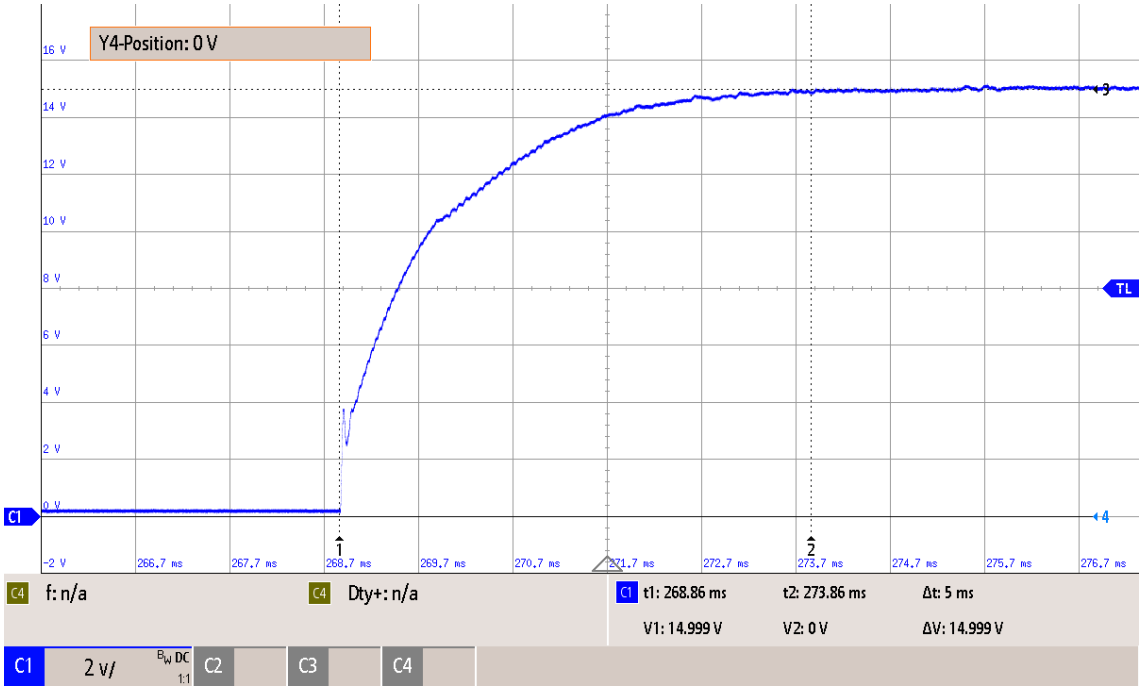

Figure 21. *Step response of Non-Inverting Buck-Boost Converter*

6. CONCLUSION

The designed and experimentally validated bi-directional non-inverting buck–boost converter exhibits a compact form factor of 20 × 37 × 9 mm (0.4 in³) and achieves a continuous output power of 135 W, corresponding to a power density of 375 W/in³. The experimental results confirm the wide input–output voltage range and demonstrate excellent conversion efficiency and high-power density. Although high-frequency output noise was initially observed during testing, the integration of a compact output filter effectively mitigated these effects. Moreover, the implementation of optimized heat dissipation techniques is expected to further enhance both efficiency and thermal reliability. A detailed correlation between simulation and experimental data confirms the accuracy of the proposed circuit model, with close agreement in output voltage behavior, noise characteristics, and efficiency, thus validating the robustness and predictability of the design.

In compliance with the ECSS-E-ST-20C standard for electrical and electronic engineering in space systems, the converter design meets key criteria for functional reliability, thermal performance, and electromagnetic compatibility, supporting its suitability for spaceborne power subsystems. Future work will aim to optimize digital control strategies to improve transient response under variable load and environmental conditions, reduce high-frequency noise through advanced EMI filtering, and enhance thermal management using improved conduction and radiation cooling paths. Further investigations will explore the scalability of this topology for higher power applications and assess the integration of other wide-bandgap devices such as SiC for radiation-tolerant and high-temperature operation. Finally, validation in representative space and aerospace system environments, including satellite power conditioning units and electric propulsion interfaces, will provide valuable data to refine the design for qualified use in space missions.

AUTHOR CONTRIBUTIONS

The article authors have contributed equally. All human authors have read and legally accepted the final version under the CC BY-SA 4.0 framework.

CONFLICT OF INTEREST

The authors declare no conflict of interest.

REFERENCES

Abdelmessih, G. Z., Alonso, J. M., Dalla Costa, M. A., Chen, Y. J., & Tsai, W. T. (2020). Fully integrated buck and boost converter as a high efficiency, high-power-density off-line LED driver. *IEEE Transactions on Power Electronics, 35*(11), 12238–12251.

Agamy, M. S., Chi, S., Elasser, A., Harfman, T. M., Jiang, Y., Mueller, F., & Tao, F. (2013). A high-power-density DC–DC converter for distributed PV architectures. *IEEE Journal of Photovoltaics, 3*(2), 791–798.

An, L., & Lu, D. D. C. (2015). Design of a single-switch DC/DC converter for a PV-battery-powered pump system with PFM+PWM control. *IEEE Transactions on Industrial Electronics, 62*(2), 910–921.

Anuraag, B. V., Mahalakshmi, R., Likhtih, S., Bhargavi, P., & Mohanty, A. (2021). *Design and comparative study of DC-DC quadratic buck-boost converter and cascaded buck-boost converter*. In: Proceedings of the International Conference on Recent Trends on Electronics, Information, Communication & Technology (RTEICT) (pp. 642–646).

Chan, C. Y. (2024). Improved voltage-mode control of a buck-boost converter based on zeta converter. *IEEE Transactions on Circuits and Systems II: Express Briefs, 71*(3), 1246–1250.

Colino, S. L., & Beach, R. A. (2009). *Fundamentals of gallium nitride power transistors (Application Note AN002).* Efficient Power Conversion.

ESA. European Space Agency. (2023). *Electrical and electronic design verification under ECSS-E-ST-20C* (Technical report).

Fleetwood, D. M., Zhang, E. X., Schrimpf, R. D., & Pantelides, S. T. (2022). Radiation effects in AlGaN/GaN HEMTs. *IEEE Transactions on Nuclear Science, 69*(5), 1105–1119.

Khuntia, M. R., & Veerachary, M. (2024). Extended boosting range-based non-isolated buck-boost converters with continuous input current and common grounded structure. *IEEE Journal of Emerging and Selected Topics in Industrial Electronics, 5*(3), 813–826.

Luo, D., Gao, Y., & Mok, P. K. T. (2022). A GaN driver for a bi-directional buck/boost converter with three-level VGS protection and optimal-point tracking dead-time control. *IEEE Transactions on Circuits and Systems I: Regular Papers, 69*(5), 2212–2224.

Luo, F., & Ma, D. (2010). Design of digital tri-mode adaptive output buck-boost power converter for power-efficient integrated systems. *IEEE Transactions on Industrial Electronics, 57*(6), 2151–2160.

Midya, P., Haddad, K., & Miller, M. (2004). Buck or boost tracking power converter. *IEEE Power Electronics Letters, 2*(4), 131–134.

Park, J. E., Han, J. K., Choi, S. H., & Moon, G. W. (2023). Two-switch forward converter with an integrated buck converter for high bus voltage in satellites. *IEEE Transactions on Power Electronics, 38*(2), 2041–2051.

Paul, R., & Maksimovic, D. (2008). *Analysis of PWM nonlinearity in non-inverting buck-boost power converters*. In: Proceedings of the IEEE Power Electronics Specialists Conference (pp. 3741–3747).

Prodic, A., & Maksimovic, D. (2002). *Design of a digital PID regulator based on look-up tables for control of high-frequency DC-DC converters*. In: Proceedings of the IEEE Workshop on Computers in Power Electronics (pp. 18–22).

Shoihet, A., & Slonim, M. A. (2012). *Analysis of transient processes of buck-boost converter: Theoretical analysis, physical experiments, modeling and simulation*. In: Proceedings of the IEEE Industrial Electronics Society Annual Conference (pp. 5365–5369).

Tsai, C. H., & Tsai, Y. S. (2014). A stable mode-transition technique for a digitally controlled non-inverting buck-boost DC-DC converter. *IEEE Transactions on Industrial Electronics, 62*(1), 475–483.

Turriate, V. O. (2018). *Design and implementation of a radiation hardened GaN-based isolated DC-DC converter for space applications* (MSc Thesis). Virginia Tech.

Ullah, B., Ullah, H., & Khalid, S. (2022). Direct model predictive control of noninverting buck-boost DC-DC converter. *CES Transactions on Electrical Machines and Systems, 6*(3), 332–339.

Veerachary, M. (2024). Bi-polar buck-boost converter. *IEEE Transactions on Circuits and Systems II: Express Briefs, 71*(4), 2429–2433.

Wai, R. J., & Shih, L. C. (2011). Design of voltage tracking control for DC-DC boost converter via total sliding-mode technique. *IEEE Transactions on Industrial Electronics, 58*(6), 2502–2511.

Wang, L., Liu, Y., Guo, Y., Wu, Q. H., & Tang, G. (2023). Stability analysis of DC-DC converters with energy balance control. *CSEE Journal of Power and Energy Systems, 9*(5), 1765–1773.

Zhang, F., Du, L., & Quian, Z. (2008). A new design method for high-power high-efficiency switched-capacitor DC–DC converters. *IEEE Transactions on Power Electronics, 23*(2), 832–840